powdered sample, and for a particular $\mathbf{Q}_\perp(\mathbf{k})$ the average value of $|\mathbf{Q}_\perp(\mathbf{k}) \wedge \hat{\lambda}|^2$ taken over the plane is $^1/_2|\mathbf{Q}_\perp(\mathbf{k})|^2$. The nuclear contributions to $\sigma_\parallel^{+-}$ and $\sigma_\perp^{+-}$ are identical, and the difference $(\sigma_\parallel^{+-} - \sigma_\perp^{+-})$ is therefore proportional to $^1/_2|\mathbf{Q}_\perp(\mathbf{k})|^2$.

The expression $|\mathbf{Q}_\perp(\mathbf{k})|^2$ may be expanded as

$$|\mathbf{Q}_\perp(\mathbf{k})|^2 = \sum_i^N \sum_j^N f^2(\mathbf{k})\, S_i S_j \sin^2 \tau\, e^{2\pi i \mathbf{r}_{ij}\cdot\mathbf{k}}$$

where $\mathbf{r}_{ij}$ is the interatomic vector between the i^{th} and j^{th} magnetic ions, τ is the angle between $\mathbf{k}$ and $\hat{\eta}$, and $f(\mathbf{k})$ is assumed to be the same for every ion. Because all possible orientations of cluster and hence of $\hat{\eta}$ are present, $|\mathbf{Q}_\perp(\mathbf{k})|^2$ must be spherically averaged. Assuming that $f(\mathbf{k})$ is spherically symmetric, the averaged value can be shown to be

$$|\mathbf{Q}_\perp(\mathbf{k})|^2 = \sum_i^N \sum_j^N S_i S_j f^2(\mathbf{k}) \left[\left(\frac{\sin(2\pi r_{ij}k)}{2\pi r_{ij}k} \right) \sin^2 \beta_{ij} - \Phi(2\pi r_{ij}k)(3\cos^2 \beta_{ij} - 1) \right]$$

where β_{ij} is the angle between $\hat{\eta}$ and $\mathbf{r}_{ij}$ and $\Phi(x) = (x\cos x - \sin x)/(x^3)$. (The equivalent Debye formula for the nuclear scattered intensity would be $|F(\mathbf{k})|^2 = \sum_i^N \sum_j^N b_i b_j [(\sin(2\pi r_{ij}k))/2\pi r_{ij}k]$.)

In the case of FeO clusters there are three trigonally equivalent directions in the (111) plane in which $\hat{\eta}$ can lie. Assuming these are equally probable, $|\mathbf{Q}_\perp(\mathbf{k})|^2$ can be averaged over these three domains to give

$$|\mathbf{Q}_\perp(\mathbf{k})|^2 = \sum_i \sum_j S_i S_j f^2(\mathbf{k}) \left[\left(\frac{\sin(2\pi k r_{ij})}{2\pi k r_{ij}} \right) \times \left(1 - \frac{1}{2}\sin^2 \delta_{ij} \right) - \Phi(2\pi k r_{ij}) \left(\frac{3}{2}\sin^2 \delta_{ij} - 1 \right) \right]$$

where δ_{ij} is the angle between $\mathbf{r}_{ij}$ and the [111] direction. Components of the spin parallel to [111] also give a contribution to the scattering, which is

$$|\mathbf{Q}_\perp(\mathbf{k})|^2 = \sum_i \sum_j [(S^2 - S_i^2)(S^2 - S_j^2)]^{1/2} f^2(\mathbf{k}) \times \left[\left(\frac{\sin(2\pi r_{ij}k)}{2\pi r_{ij}k} \right) \sin^2 \delta_{ij} - \Phi(2\pi k r_{ij})(3\cos^2 \delta_{ij} - 1) \right]$$

where S is the full spin associated with the iron atoms. A more reasonable assumption in this case is that the axial components are coherent with those parallel to [111] in the nearby clusters, in which case, by employing Babinet's principle it can be shown that the term $[(S^2 - S_i^2)(S^2 - S_j^2)]^{1/2}$ in the above expression should be replaced by $[S - (S^2 - S_i^2)^{1/2}][S - (S^2 - S_j^2)^{1/2}]$.

Registry No. Wüstite, 17125-56-3.

Contribution from the Department of Chemistry, University of Missouri—Rolla, Rolla, Missouri 65401, Chemical Crystallography Laboratory, Oxford University, Oxford OX1 3PD, England, and Nuclear Physics Division, Atomic Energy Research Establishment, Harwell, Didcot OX11 0RA, England

Neutron Diffraction and Mössbauer-Effect Study of $(Mn_xFe_{1-x})_yO$ Solid Solutions

GARY J. LONG,* D. A. O. HOPE, and A. K. CHEETHAM*

Received September 15, 1983

The nonstoichiometric solid solutions $(Mn_xFe_{1-x})_yO$ have been studied at low temperatures by Mössbauer spectroscopy and Rietveld analysis of powder neutron diffraction data. For $x < 0.23$, the neutron measurements show that the spin direction is between the [111] axis and the (111) plane, as in Fe_yO itself, but for $x > 0.23$ the spins appear to lie in the (111) plane. Except for samples with y close to unity, the coherent magnetic scattering is less than expected, indicating that long-range magnetic ordering is not complete. The Mössbauer spectra of samples containing large concentrations of iron(III) are very complex and are fitted to a model with three hyperfine sextets, two for octahedral iron(II) and one for octahedral iron(III), and a quadrupole doublet for tetrahedral iron(III). For samples containing almost no iron(III), the spectra were fitted to a model with three iron(II) sextets, corresponding to sites with differing numbers of manganese neighbors.

Introduction

The monoxides of manganese and iron adopt the rock salt structure and are completely miscible at temperatures above 900 °C, as illustrated in the phase diagram[1] presented in Figure 1. Iron(II) oxide is nonstoichiometric, accommodating a deficiency of iron by the formation of iron vacancies and a small number of iron interstitials.[2] These defects aggregate to form the tetrahedral units[3] shown in Figure 2a, which are believed to condense by edge sharing to form larger units such as the 6:2 vacancy to interstitial cluster[4] shown in Figure 2b. Below 570 °C, iron(II) oxide disproportionates into iron metal and Fe_3O_4.[5] The solid solutions, $(Mn_xFe_{1-x})_yO$, can be quenched to room temperature, and our recent examination of these materials by neutron diffraction and Mössbauer spectroscopy has shown that their defect structure is similar to that of Fe_yO, itself.[6]

On cooling below room temperature, Fe_yO and MnO become antiferromagnetically ordered with Néel temperatures of ca. 200 and 118 K, respectively.[7,8] In both cases, the onset of magnetic ordering is accompanied by a rhombohedral distortion, which may be expressed in terms of the rhombohedral distortion angle, α; Fe_yO has α less than 90° and the spin apparently directed along the [111] axis,[9] whereas MnO has α greater than 90° with the spin lying in the (111) plane.[10]

* To whom correspondence should be addressed: G.J.L., University of Missouri—Rolla; A.K.C., Oxford University.

(1) Tret'yakov, Y. D.; Saksonov, Y. G.; Gordeev, I. V. *Inorg. Mater.* (*Engl. Transl.*) **1965**, *1*, 382.
(2) Roth, W. L. *Acta Crystallogr.* **1960**, *13*, 40.
(3) Cheetham, A. K.; Fender, B. E. F.; Taylor, R. I. *J. Phys. C* **1971**, *4*, 2160.
(4) Catlow, C. R. A.; Fender, B. E. F. *J. Phys. C* **1975**, *8*, 3267.
(5) Fender, B. E. F.; Riley, F. D. *J. Phys. Chem. Solids* **1969**, *30*, 793.
(6) Hope, D. A. O.; Cheetham, A. K.; Long, G. J. *Inorg. Chem.* **1982**, *21*, 2804.
(7) Koch, F.; Fine, M. E. *J. Appl. Phys.* **1966**, *38*, 1470.
(8) Boire, R.; Collins, M. F. *Can. J. Phys.* **1977**, *55*, 688.
(9) Shull, C. G.; Strauser, W. A.; Wollan, E. O. *Phys. Rev.* **1951**, *83*, 333.
(10) Bidaux, R.; Conte, R.; Nasser, J. A. *J. Phys.* (*Orsay, Fr.*) **1980**, *41*, 1317.

0020-1669/84/1323-3141$01.50/0

Table I. Summary of Neutron Diffraction Results for $(Mn_xFe_{1-x})_yO$ Obtained at 4.2 K

compd	a (=b = c), Å	deg[e] α	deg[e] β	deg[e] γ	overall B factor, Å^2	R_{pr},[a] %	R_{mag}, %	μ,[b] μ_B	θ,[c] deg	instrument	wavelength, Å
$Fe_{0.938}O$	8.513 (1)	89.65	89.65	89.65	0.72 (6)	13.3	14.4	2.0 (2)	0	Panda	1.3
$(Mn_{0.05}Fe_{0.95})_{0.954}O$	8.614 (1)	89.76	89.76	89.76	0.62 (3)	9.87	7.82	3.1 (1)	0	Curran	1.4
$(Mn_{0.05}Fe_{0.95})_{0.936}O$	8.634 (1)	90.00	90.00	90.00	0.52 (4)	6.97	14.87	3.1 (1)	3	D1A	1.5
$(Mn_{0.10}Fe_{0.90})_{0.931}O$	8.622 (1)	90.00	90.00	90.00	0.78 (5)	9.66	9.98	3.0 (3)	29	Panda	1.5
$(Mn_{0.12}Fe_{0.88})_{0.926}O$	8.624 (1)	90.05	90.05	90.05	0.86 (3)	7.25	10.04	3.0 (1)	50	D1A	1.5
$(Mn_{0.23}Fe_{0.77})_{0.929}O$	8.646 (1)	90.03	90.03	90.03	0.71 (4)	6.70	10.52	3.2 (1)	90	Panda	1.5
$(Mn_{0.36}Fe_{0.64})_{0.954}O$	8.712 (1)	90.05	90.05	90.05	0.90 (3)	9.07	8.96	3.5 (1)	90	D1A	1.5
$(Mn_{0.56}Fe_{0.44})_{0.993}O$	8.780 (1)	90.15	90.15	89.94	0.59 (2)	4.89	1.95	4.0 (1)	90	D1A	1.5
$(Mn_{0.66}Fe_{0.34})_{0.954}O$	8.754 (1)	90.08	90.08	90.08	1.25 (10)	19.59[d]	14.25[d]	3.7 (1)	90	D1A	1.9
$(Mn_{0.89}Fe_{0.11})_{0.997}O$	8.854 (1)	90.58	90.58	90.58	0.51 (6)	10.65	7.93	4.4 (1)	90	Panda	1.5
MnO	8.864 (1)	90.61	90.61	90.61	0.25 (2)	7.04	2.75	4.6 (1)	90	D1A	1.5

[a] The definitions of R_{pr} and R_{mag} are given by Rietveld.[18] [b] The mean magnetic moment per occupied octahedral site. [c] The angle between the spin direction and the [111] direction. [d] A refinement of this data without a composition constraint[6] gave a R_{pr} of 15.1%. [e] The esd's on the angles are 0.01°.

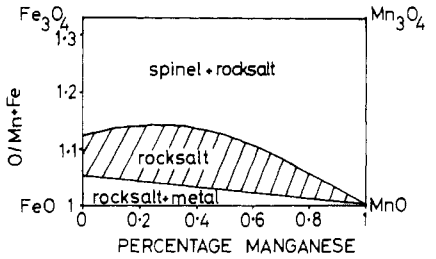

Figure 1. Phase diagram for the $(Mn_xFe_{1-x})_yO$ solid solutions.

In the case of Fe_yO, the spin direction and rhombohedral distortion are controlled by the single-ion anisotropy of the orbitally degenerate iron(II) ion,[11] although the spin direction rotates from close to the (111) plane in the vicinity of the defect clusters toward the [111] axis between the clusters.[12] The component of spin in the (111) plane is only ordered over short distances, leading to the absence of a coherent, {111} magnetic reflection.[13] In MnO, the spin direction is determined by dipole–dipole interactions and the rhombohedral symmetry is a result of direct manganese(II)–manganese(II) exchange.[14]

We have recently described the competing magnetic anisotropies in the solid solutions $(Co_xNi_{1-x})O$[15] and $(Mn_xNi_{1-x})_yO$,[16] and we find in both systems that the spin structures are collinear. In this paper we describe the low-temperature behavior of the more complex system, $(Mn_xFe_{1-x})_yO$, as determined by neutron diffraction and Mössbauer-effect measurements. The Néel temperature is known to be a linear function of composition,[17] but the variations in crystal symmetry, spin direction, magnetic moment, and internal hyperfine field have not been determined previously.

Experimental Section

The samples were prepared, characterized, and analyzed by the methods reported previously.[6] X-ray powder diffraction studies indicated the absence of Fe_3O_4, and only lines attributable to Fe_yO were observed.

Mössbauer-effect absorbers were prepared by mixing fine powders with Vaseline to remove any potential crystallite orientation effects and contained ca. 50 mg of sample/cm^2. The spectra were obtained on either a Ranger Electronics or a Harwell constant-acceleration spectrometer, each of which used a room-temperature rhodium-matrix source and was calibrated at room temperature with natural α-iron foil. Liquid-helium-temperature spectra were obtained in a cryostat in which the samples were placed directly into liquid helium. Least-squares minimization programs implemented on the Amdahl 7 at the University of Missouri—Rolla were used to analyze the spectra.

Neutron powder diffraction profiles were recorded at 4.2 K on the diffractometers D1A at the ILL, Grenoble, France, and Panda and Curran at the AERE, Harwell, England. Experimental details of the data refinement[18] and the line profile analysis are presented elsewhere,[6] and results are presented in Table I. Typical profiles are shown in Figure 3.

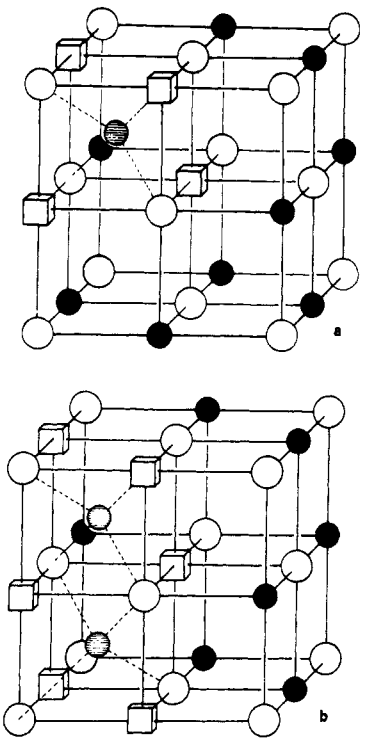

Figure 2. Defect clusters in Fe_yO: (a) an isolated 4:1 cluster; (b) a 6:2 cluster with a common shared edge. Filled circles are octahedral iron atoms, shaded circles are tetrahedral iron interstitials, open circles are oxygen atoms, and cubes are octahedral vacancies.

Results and Discussion

Neutron Diffraction Data. The most striking feature of the neutron diffraction patterns obtained at 4.2 K is the appearance of a {111} magnetic reflection when as little as 5% manganese is doped into Fe_yO, as illustrated in Figure 4; this reflection is entirely absent in pure iron(II) oxide. Refinements

(11) Kanamori, J. *Prog. Theor. Phys.* **1957**, *17*, 197.
(12) Battle, P. D.; Cheetham, A. K. *J. Phys. C* **1979**, *12*, 337.
(13) Wilkinson, C.; Cheetham, A. K.; Long, G. J.; Battle, P. D.; Hope, D. A. O. *Inorg. Chem.*, preceding paper in this issue.
(14) Kaplan, J. I. *J. Chem. Phys.* **1954**, *22*, 1709.
(15) Battle, P. D.; Cheetham, A. K.; Gehring, G. A. *J. Appl. Phys.* **1979**, *50*, 7578.
(16) Cheetham, A. K.; Hope, D. A. O. *Phys. Rev. B* **1983**, *27*, 6964.
(17) Evrard, O. *Rev. Chim. Miner.* **1971**, *8*, 63.
(18) Rietveld, H. M. *J. App. Crystallogr.* **1969**, *2*, 65.

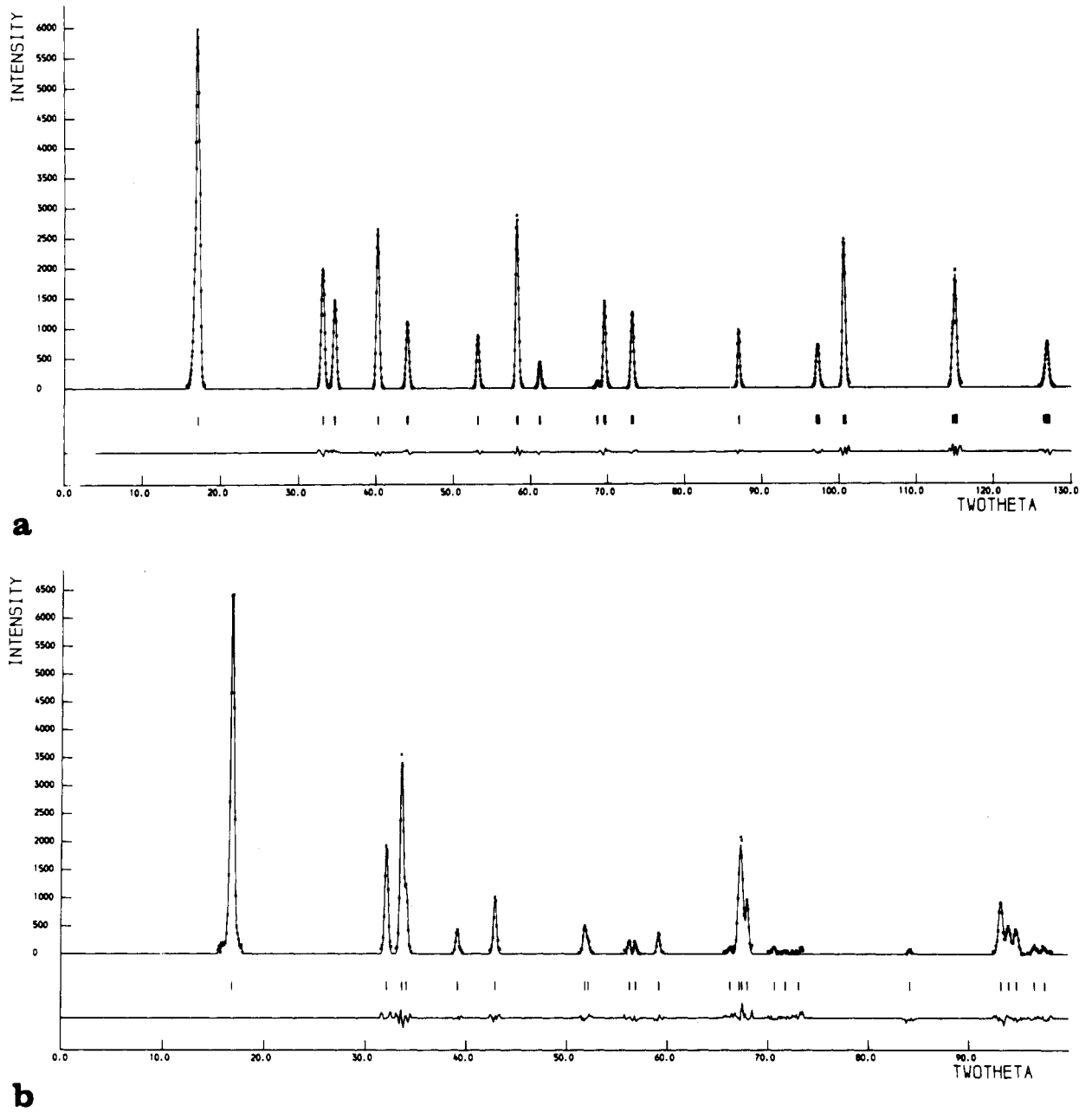

Figure 3. Observed (points) and calculated (line) powder neutron profiles obtained at 5 K for (a) $(Mn_{0.56}Fe_{0.44})_{0.993}O$ and at 4.2 K for (b) $(Mn_{0.89}Fe_{0.11})_{0.997}O$. A difference curve and the positions of the Bragg reflections are shown below the profile, which includes both magnetic and nuclear reflections. The reduction in symmetry is clearly evident in part b.

of the neutron data for the solid solutions included in Table I show that the spin rotates into the (111) plane as manganese is added to Fe_yO and that the rotation is complete after the addition of only 23% manganese. The change in spin direction is accompanied by a dramatic reduction in the magnitude of the $\alpha < 90°$ rhombohedral distortion, and the symmetry is essentially cubic, or pseudocubic, until the $\alpha > 90°$ distortion emerges at very high manganese contents (see Table I). The third significant feature of the neutron results is the variation in the cation moment per *occupied* octahedral site as a function of composition. Figure 5 shows that this quantity falls well below the values expected for a collinear magnetic structure, whether the orbital angular momentum of the iron(II) ion is sustained or quenched; a spin-only magnetic moment of 3.6 μ_B was assumed for iron(II), a spin-plus orbital magnetic moment of 4.2 μ_B was assumed for iron(II), and a moment of 4.6 μ_B was assumed for manganese(II).

The diminution of the $\alpha < 90°$ rhombohedral distortion in the 0–23% manganese composition range is similar to the effect observed in Fe_yO when the degree of nonstoichiometry is increased,[19] i.e., y is decreased; in both instances, a high-spin d^5 ion, manganese(II) or iron(III), is introduced into the structure. In Fe_yO, the rhombohedral distortion disappears when y is approximately 0.89, corresponding to approximately 25 atm % iron(III).[19] The changes observed are more pronounced than would be expected solely on account of the reduction of the concentration of iron(II) with its associated magnetostriction, and we must conclude that a competing interaction, favoring $\alpha > 90°$, is present. Obvious candidates for this interaction are Fe^{3+}–Fe^{3+} exchange in Fe_yO and Mn^{2+}–Fe^{2+} and Mn^{2+}–Mn^{2+} exchange in the solid solutions, all of which are antiferromagnetic;[20] Fe^{2+}–Fe^{2+} exchange is ferromagnetic when α is less than 90° and antiferromagnetic otherwise.[21]

(19) Willis, B. T. M.; Rooksby, H. P. *Acta Crystallogr.* **1953**, *6*, 827.
(20) Goodenough, J. B. *Phys. Rev.* **1955**, *100*, 564; **1960**, *117*, 1442; *J. Phys. Chem. Solids* **1958**, *6*, 287. Kanamori, J. *Ibid.* **1959**, *10*, 87.

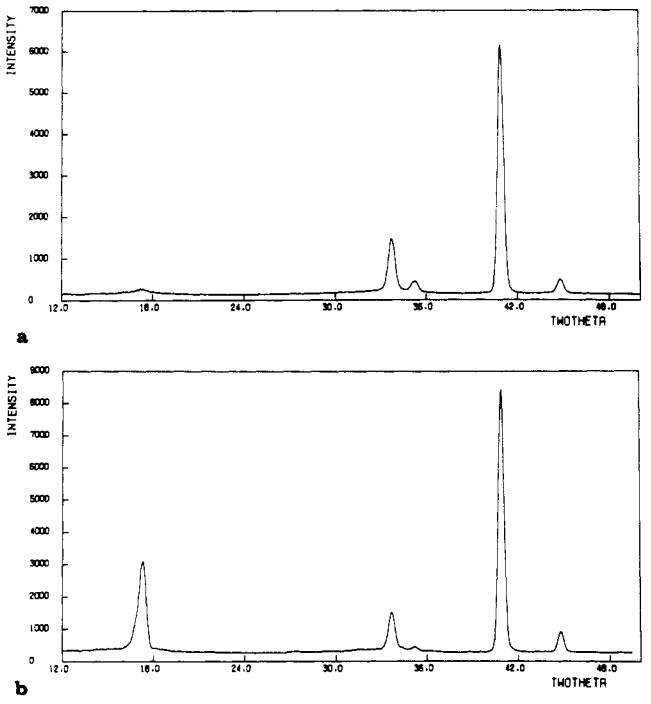

Figure 4. Low-angle regions of the powder neutron diffraction patterns of (a) $(Mn_{0.05}Fe_{0.95})_{0.954}O$ and (b) $(Mn_{0.12}Fe_{0.88})_{0.926}O$, showing the increase in the intensity of the {111} magnetic reflection at $2\theta = 17°$ with increasing manganese(II) content.

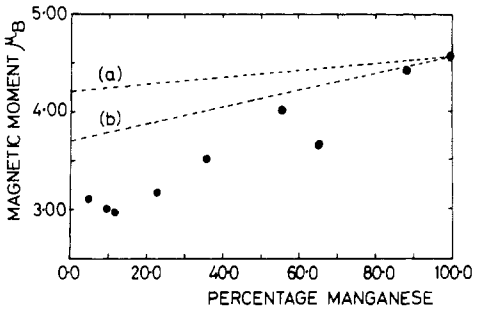

Figure 5. Plot of the magnetic moment vs. composition for the $(Mn_xFe_{1-x})_yO$ solid solutions. Line a represents the predicted variation for a collinear model in which the orbital angular momentum of iron(II) is sustained, and line b shows the variation for quenched iron(II).

The single-ion anisotropy of iron(II) is lost in samples containing more than 23% manganese because it requires a component of spin along the [111] direction. It is surprising, therefore, to find that the deviations from cubic symmetry are so small over a wide range of composition in $(Mn_xFe_{1-x})_yO$. In this respect, the results are similar to those found in $(Mn_xNi_{1-x})O$, where antiferromagnetic Mn^{2+}–Mn^{2+} exchange is balanced by ferromagnetic Mn^{2+}–Ni^{2+} interactions.[16] In manganowüstite, the > 90° distortion results from the antiferromagnetic exchange strictions described above and the Jahn–Teller stabilization of iron(II). The origin of the ferromagnetic < 90° exchange striction is unclear, but one possibility is a 90° cation–cation exchange mechanism similar to that found in NiO.[22]

The rotation of the spin direction into the (111) plane in the range of 0–23% manganese is interesting because it indicates that the single-ion anisotropy of iron(II) is not as strong as would be expected by comparison with other systems, for example $K_2Mn_{1-x}M_xF_4$, where M is Fe and Co.[23] It is

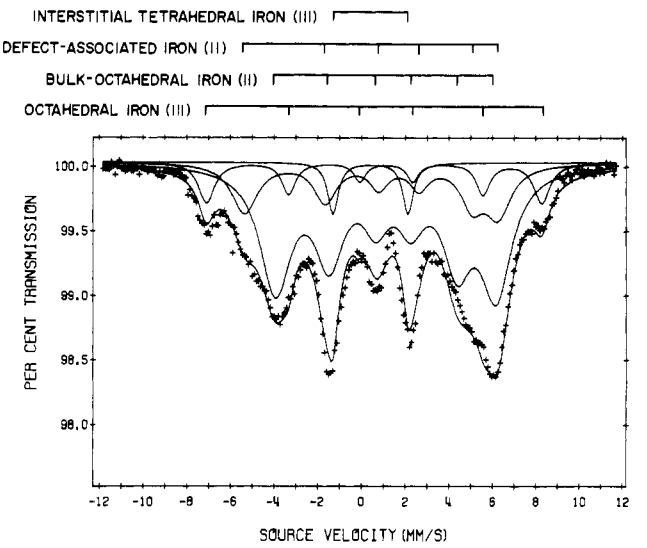

Figure 6. Mössbauer-effect spectrum of $(Mn_{0.36}Fe_{0.64})_{0.954}O$ obtained at 78 K.

probable that the iron(II) spin direction is genuinely tilted from the [111] axis in this composition range, and the iron and manganese spins lie closer to the (111) plane in the vicinity of the defects. The latter situation exists in Fe_yO, but the domains in which the planar spin component is ordered are sufficiently small (ca. 80 Å in diameter) that coherent scattering into the {111} magnetic reflection is not observed.[13] The emergence of a {111} reflection when as little as 5% manganese is added to Fe_yO is indicative of a larger domain size. For manganese contents of more than 23%, the {111} reflection is a consequence of an ordered spin component lying entirely within the (111) plane.

As in Fe_yO,[2,12] the coherent magnetic scattering is less than that predicted for a collinear model in which all the cations are contributing (see Figure 5), except for the samples with compositions close to the stoichiometric solid solution, $(Mn_xFe_{1-x})_yO$, where y is essentially 1. In the latter cases, at 56 and 89% manganese, the observed moments are in reasonable agreement with those expected if the orbital angular momentum of iron(II) is quenched, as suggested above. The shortfall in the average magnetic moments for the nonstoichiometric samples is apparent, even when the spins lie in the (111) plane, i.e. for >23 mol % MnO. This suggests that the planar spin component is incompletely ordered, even when the spin direction lies entirely within the (111) plane. An alternative interpretation is that for manganese contents greater than 23 mol %, the spins do not lie completely in the (111) plane but the axial spin components are not fully ordered.

Finally we note that for $(Mn_{0.56}Fe_{0.44})_{0.993}O$, consistency between the nuclear and magnetic periodicities requires a monoclinic cell with $a = b \approx c$, $\alpha = \beta > 90°$, and $\delta < 90°$ as shown in Table I. This result suggests that the magnetic structure does not propagate along a 3-fold axis. A similar anomaly was reported for $(Mn_{0.77}Ni_{0.23})O$,[16] but we have no convincing explanation to offer for this effect.

Mössbauer-Effect Spectral Data. The room-temperature Mössbauer spectra of the series of compounds, $(Mn_xFe_{1-x})_yO$, have been reported previously[6] and reveal an iron(III) absorption singlet and up to three doublets which were attributed to iron(II) in various sites. The Mössbauer spectra of each of these materials have now been measured at 78 and 4.2 K. The results may be divided into two categories. First are those with a large amount of iron(III), which exhibit very complex

(21) Goodenough, J. B. *Phys. Rev.* **1968**, *171*, 466.
(22) Hope, D. A. O. D.Phil. Thesis, Oxford University, 1981.
(23) Bevaart, L.; Frikkee, E.; Levesque, J. V.; de Jongh, L. J. *Phys. Rev. B* **1978**, *18*, 33.

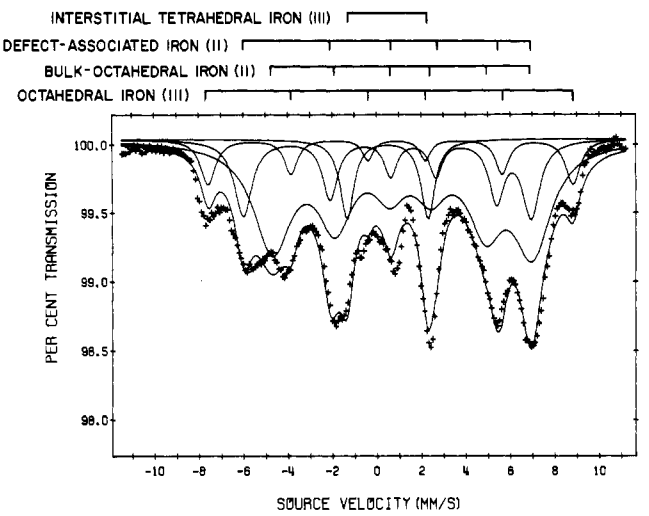

Figure 7. Mössbauer-effect spectrum of $(Mn_{0.36}Fe_{0.64})_{0.954}O$ obtained at 4.2 K.

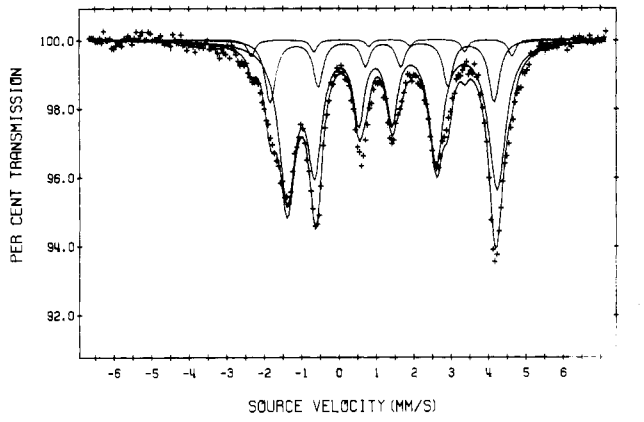

Figure 8. Mössbauer-effect spectrum of $(Mn_{0.975}{}^{57}Fe_{0.025})_{0.998}O$ obtained at 78 K.

magnetic spectra as is illustrated for $(Mn_{0.36}Fe_{0.64})_{0.954}O$ at 78 K in Figure 6 and at 4.2 K in Figure 7. The second category includes materials that are low in iron(III) and have a high manganese(II) to iron(II) ratio. These materials exhibit a broad six-line Mössbauer spectrum, as is illustrated for $(Mn_{0.975}{}^{57}Fe_{0.025})_{0.998}O$ at 78 K in Figure 8.

The $(Mn_xFe_{1-x})_yO$ compounds in the first category exhibit Mössbauer spectra that are quite similar to those obtained for Fe_yO.[13] The spectra are very complex, and repeated attempts to fit these results in terms of a range of magnetic sextets always failed because it was impossible to fit the strong lines found at ca. −1.5 and 2.5 mm/s, exactly as was found in the case of $Fe_{0.918}O$. The inclusion of a quadrupole doublet, to account for these two lines, and three constrained[24] magnetic sextets led immediately to acceptable fits to the experimental spectra that seem chemically reasonable. In each case the area of the quadrupole doublet corresponded approximately to that expected from the tetrahedral interstitial iron(III). The resulting fits are shown in Figures 6 and 7, and the spectral parameters are presented in Table II. In these fits the relative areas of each separate spectral component were calculated on

(24) Each magnetic sextet was fitted on the basis of an adjustable isomer shift, δ, internal hyperfine field, H_{int}, quadrupole shift, QS, and line width, Γ, which was the width of the outer and magnetic lines, lines 1 and 6. The line widths of lines 2 and 5 were $\Gamma - 0.5\Delta\Gamma$, and the line widths of lines 3 and 4 were $\Gamma - \Delta\Gamma$, where $\Delta\Gamma$ was determined from preliminary fits and was not refined. The relative areas of the lines in each sextet were constrained in the ratio of 3:2:1:1:2:3 as required for an unoriented powder sample. Each component of the quadrupole doublet was constrained to have the same area and line width.

Table II. Mössbauer-Effect Spectral Parameters for a Series of $(Mn_xFe_{1-x})_yO$ Solid Solutions[a]

compd	T, K	octahedral iron(III)						defect-associated iron(II)						bulk iron(II)						interstitial iron(III)						
		δ	QS	H_{int}	Γ	$\Delta\Gamma$	% A	δ	QS	H_{int}	Γ	$\Delta\Gamma$	% A	δ	QS	H_{int}	Γ	$\Delta\Gamma$	% A	δ	ΔE_Q	Γ	% A	χ^2
$Fe_{0.918}O$	78	0.86	+0.20	495	0.83	0.24	12.5	1.07	+0.59	400	1.44	0.41	23.1	1.26	−0.01	355	2.23	0.37	59.0	0.43	3.84	0.62	5.4	3.40
	4.2	0.81	+0.21	510	0.70	0.20	12.5	1.03	+0.63	421	1.29	0.37	23.1	1.30	+0.05	380	2.39	0.40	59.0	0.37	3.98	0.59	5.4	4.55
$(Mn_{0.10}Fe_{0.90})_{0.913}O$	78	0.85	+0.17	492	0.87	0.24	12.3	1.14	+0.56	397	1.05	0.31	17.0	1.24	+0.06	348	2.08	0.36	66.7	0.47	3.82	0.45	4.0	2.37
	4.2	0.83	+0.19	503	0.88	0.25	12.3	1.14	+0.55	418	0.91	0.25	17.0	1.32	+0.08	372	2.52	0.42	66.7	0.37	3.97	0.41	4.0	3.34
$(Mn_{0.23}Fe_{0.77})_{0.929}O$	78	0.79	+0.15	488	0.96	0.27	15.4	1.06	+0.50	390	1.50	0.42	22.7	1.30	+0.19	336	1.99	0.32	57.6	0.47	3.48	0.60	4.3	5.79
	4.2	0.71	+0.06	505	0.96	0.28	15.4	1.13	+0.57	415	1.29	0.37	22.7	1.26	+0.12	369	2.49	0.41	57.6	0.43	3.86	0.49	4.3	3.98
$(Mn_{0.36}Fe_{0.64})_{0.954}O$	78	0.85	+0.26	476	0.88	0.25	10.6	1.08	+0.62	360	1.44	0.42	21.3	1.29	+0.16	313	1.74	0.29	63.7	0.41	3.42	0.58	4.4	3.19
	4.2	0.74	+0.11	507	0.84	0.24	10.6	1.07	+0.58	400	0.97	0.28	21.3	1.34	+0.19	358	2.16	0.36	63.7	0.48	3.64	0.42	4.4	10.57
$(Mn_{0.66}Fe_{0.34})_{0.954}O$	78	0.55	−0.02	467	0.90	0.25	21.2	1.02	+0.48	369	2.23	0.64	35.4	1.20	+0.15	259	1.41	0.24	36.4	0.56	3.07	0.96	7.1	1.73
	4.2	0.51	−0.01	506	0.79	0.23	21.2	1.03	+0.53	392	2.44	0.70	35.4	1.32	+0.02	315	1.90	0.32	36.4	0.75	3.02	0.82	7.1	1.83
$(Mn_{0.10}{}^{57}Fe_{0.90})_{0.997}O^b$	78	*c*						1.23	−0.08	206	0.79	0.42	42.4	1.27	−0.35	190	0.88	0.51	31.9	*c*				3.12
								1.36	+0.14	238	0.91	0.38	25.8											
$(Mn_{0.975}{}^{57}Fe_{0.025})_{0.998}O^b$	78	*c*						1.17	+0.01	186	0.37	0.07	22.4	1.20	−0.22	174	0.52	0.17	73.9	*c*				3.72
								1.27	+0.04	221	0.24	0.04	3.6											

[a] All data except H_{int} in mm/s relative to room-temperature natural α-iron foil. H_{int} is in kOe. The constraints imposed upon each component are given in footnote 24. The relative area of each component was constrained as discussed in the text. [b] For these compounds the relative areas were constrained to the values obtained from a binomial calculation of the number of iron(II) near neighbors (see text and footnote 6). [c] Component not observed.

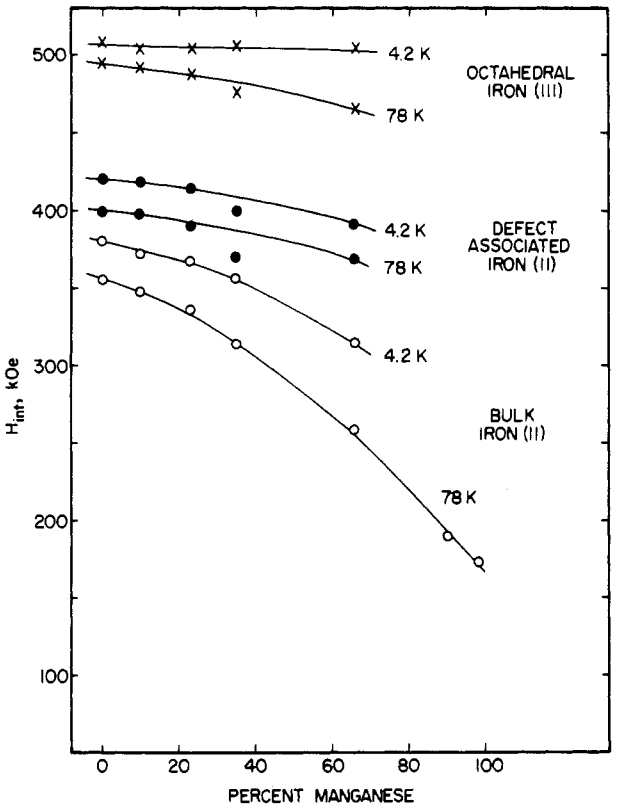

Figure 9. Internal hyperfine field vs. composition for the $(Mn_xFe_{1-x})_yO$ solid solutions.

the basis of a 6:2 cluster (Figure 2b), from the stoichiometry of the compound as determined by chemical analysis, and the vacancy concentration obtained from the neutron diffraction results.[6] If this relative area constraint was removed, there was little change in the hyperfine parameters but there was a tendency to decrease the relative area of the sextet attributed to the bulk iron(II). The spectral parameters obtained for these area unconstrained fits are presented in Tables III and IV (supplementary material).

The fits obtained in our analysis of these spectra are far from exact, and in most cases the line widths for the magnetic components are quite high. However, they provide an excellent starting point for a discussion of the magnetic properties of these complex nonstoichiometric oxides. The three magnetic components may be assigned to substitutional iron ions with different local environments. On the basis of its relative area and the size of the internal field, the component with the largest H_{int} is assigned to the substitutional octahedral iron(III), which is mainly associated with the interstitial clusters to provide charge neutrality. The nearby vacancies and their resulting large lattice contribution to the electric field gradient tensor at the iron(III) ion account for the fairly large quadrupole shift observed for this component. The second magnetic component is assigned to the iron(II) ion that is closely associated with the defect cluster and hence has a higher internal hyperfine field than "bulk" iron(II). Again the interstitial iron(III) and its associated vacancies produce the large observed quadrupole shift found for this component. The third magnetic component, with a small quadrupole shift, is assigned to the iron(II) in the bulk of these rock salt like oxides. Both of the iron(II) components have isomer shifts that are typical of high-spin iron(II) and large line widths reflecting the presence of the defect clusters and varying numbers of near-neighbor manganese(II) ions.

As for Fe_yO,[13] the $(Mn_xFe_{1-x})_yO$ spectra contain a symmetric quadrupole doublet that appears in each of the materials in which y is significantly less than 1. It is thus apparent that this component must be closely associated with the defect clusters (Figure 2) found in these oxides. As noted below, no such component is found in the essentially defect-free stoichiometric materials. On the basis of its isomer shift (ca. 0.4 mm/s) and its relative area, this component is assigned to the interstitial tetrahedral iron(III) ion in the defect clusters. Again, a large quadrupole splitting of ca. 3–4 mm/s is found for this component. It has a much smaller splitting at room temperature, and the enhanced splitting at low temperature results from both the distortion arising from magnetic ordering around the cluster below T_N and the decreased importance of iron(II)–iron(III) electron transfer at low temperature. Both of these processes would serve to increase the electric field gradient tensor at the interstitial iron(III) site at low temperature. As in Fe_yO, the interstitial is either paramagnetic or spin paired with adjacent interstitials.

The second category of compounds is that of the essentially defect-free oxides represented by $(Mn_{0.90}{}^{57}Fe_{0.10})_{0.997}O$ and $(Mn_{0.975}{}^{57}Fe_{0.025})_{0.998}O$. The Mössbauer spectrum of the latter compound is illustrated in Figure 8 and reveals the presence of three magnetic components that may be attributed to the 73.9% of the iron-57 ions that have 12 near-neighbor manganese(II) ions and the 22.5% of the iron-57 ions that have 11 manganese(II) and 1 iron(II) near neighbors; only 3.6% of the iron-57 ions would have 2 or more near-neighbor iron(II) ions.[6] It should be noted that in this case there is no magnetic sextet that could be attributed to iron(III) and there is no evidence for the quadrupole doublet that was attributed above to the interstitial tetrahedral iron(III) ion in the defect cluster.

The study of the series of compounds with differing manganese content permits us to evaluate the internal hyperfine field as a function of the iron environment. The internal hyperfine field as a function of manganese content for each of the magnetic sextets is presented in Figure 9. As expected, the internal hyperfine field of the octahedral substitutional iron(III) is essentially saturated at ca. 505 kOe at 4.2 K, a value that is substantially reduced from the ideal 550 kOe value[25] by the extensive covalency in the bonding in Fe_yO type materials. There is little change in H_{int} at 4.2 K with increasing manganese content because of the preference of the substitutional octahedral iron(III) for the defect cluster, thereby excluding to some extent the manganese(II) from the vicinity of the cluster. The internal hyperfine field of the defect-associated iron(II) and the octahedral iron(III) at 78 K decreases slightly with increasing manganese content because of the decrease in T_N from ca. 200 K at 0% manganese to ca. 140 K at 70% manganese. The decrease in internal hyperfine field with increasing manganese content is largest for the iron(II) site assigned to the bulk rock salt like environment. In this case, the decreasing T_N, the increasing covalence of the Fe–O bond in the presence of the more numerous manganese(II) ions, and any transferred hyperfine field from the antiferromagnetically coupled manganese(II) ions will tend to decrease the internal hyperfine field.

Acknowledgment. It is a pleasure to acknowledge the assistance and helpful discussions with Drs. T. E. Cranshaw, A. Gérard, F. Grandjean, G. Longworth, A. W. Hewat and B. Laundy. We thank the Science and Engineering Research Council for the provision of the neutron facilitites at ILL, Grenoble, and a research studentship for D.A.O.H., NATO for a cooperative scientific research grant, and the USAF for a support grant (AFOSR-79-0120).

Supplementary Material Available: Tables III and IV, giving Mössbauer-effect spectral parameters for $(Mn_xFe_{1-x})_yO$ (2 pages). Ordering information is given on any current masthead page.

(25) Johnson, C. E. In "Hyperfine Interactions in Excited Nuclei"; Goldring, G., Kalish, R., Eds.; Gordon and Breach: New York, 1971.